RESEARCH ARTICLE

# PAX3–FOXO1 Establishes Myogenic Super Enhancers and Confers BET Bromodomain Vulnerability

Berkley E. Gryder[1], Marielle E. Yohe[1,2], Hsien-Chao Chou[1], Xiaohu Zhang[3], Joana Marques[4], Marco Wachtel[4], Beat Schaefer[4], Nirmalya Sen[1], Young Song[1], Alberto Gualtieri[5], Silvia Pomella[5], Rossella Rota[5], Abigail Cleveland[1], Xinyu Wen[1], Sivasish Sindiri[1], Jun S. Wei[1], Frederic G. Barr[6], Sudipto Das[7], Thorkell Andresson[7], Rajarshi Guha[3], Madhu Lal-Nag[3], Marc Ferrer[3], Jack F. Shern[1,2], Keji Zhao[8], Craig J. Thomas[3], and Javed Khan[1]

**ABSTRACT** Alveolar rhabdomyosarcoma is a life-threatening myogenic cancer of children and adolescent young adults, driven primarily by the chimeric transcription factor PAX3–FOXO1. The mechanisms by which PAX3–FOXO1 dysregulates chromatin are unknown. We find PAX3–FOXO1 reprograms the *cis*-regulatory landscape by inducing *de novo* super enhancers. PAX3–FOXO1 uses super enhancers to set up autoregulatory loops in collaboration with the master transcription factors MYOG, MYOD, and MYCN. This myogenic super enhancer circuitry is consistent across cell lines and primary tumors. Cells harboring the fusion gene are selectively sensitive to small-molecule inhibition of protein targets induced by, or bound to, PAX3–FOXO1-occupied super enhancers. Furthermore, PAX3–FOXO1 recruits and requires the BET bromodomain protein BRD4 to function at super enhancers, resulting in a complete dependence on BRD4 and a significant susceptibility to BRD inhibition. These results yield insights into the epigenetic functions of PAX3–FOXO1 and reveal a specific vulnerability that can be exploited for precision therapy.

**SIGNIFICANCE:** PAX3–FOXO1 drives pediatric fusion-positive rhabdomyosarcoma, and its chromatin-level functions are critical to understanding its oncogenic activity. We find that PAX3–FOXO1 establishes a myoblastic super enhancer landscape and creates a profound subtype-unique dependence on BET bromodomains, the inhibition of which ablates PAX3–FOXO1 function, providing a mechanistic rationale for exploring BET inhibitors for patients bearing PAX-fusion rhabdomyosarcoma. *Cancer Discov; 7(8); 884–99. ©2017 AACR.*

## INTRODUCTION

Transcription factors (TF) recognize specific noncoding sequences across the genome, recruiting epigenetic machinery to regulate key cell identity genes, and are sequentially exchanged during development and differentiation (1). Oncogenic fusion genes involving TFs are predicted to profoundly alter normal developmental progression and cell identity in many malignancies (2).

Rhabdomyosarcoma (RMS) is a cancer of childhood and adolescence characterized by its inability to exit the proliferative myoblast-like state. Genomic and transcriptomic characterization implicates either chromosomal translocation resulting in the oncogenic fusion transcription factor PAX3/7–FOXO1 (fusion-positive alveolar subtype, FP-RMS) or mutations in receptor tyrosine kinase/RAS pathways (fusion-negative embryonal subtype, FN-RMS; refs. 3, 4). FP-RMS is characterized by a strikingly low somatic mutational burden indicating that the fusion gene is the primary oncogenic driver. Many other transcription/chromatin factor fusion gene–driven sarcomas have similar low mutational burdens (5–7). Importantly, patients with RMS who harbor a PAX3 fusion are more likely to be metastatic at presentation, relapse despite aggressive therapy, and have very poor survival (8), underscoring the critical need to develop therapeutic strategies for this subset of patients.

Early (PAX family TFs) and late (MYOG) regulators of normal myogenesis are temporally mutually exclusive in normal muscle development, yet FP-RMS tumors concurrently express high levels of PAX3–FOXO1 and the myogenic MYOD, MYOG, as well as MYCN (9, 10). Although the transcriptional perturbation caused by the PAX fusions has been previously reported (11, 12), the chromatin mechanisms by which PAX fusions dysregulate the myogenic program are unknown. In this work, we interrogated the underlying epigenetics that enforce the myogenic and oncogenic transcriptional program of cell lines and clinical tumor samples with PAX3 fusions. In charting the genome-wide landscape of histone modifications, we discovered that PAX3–FOXO1 drives expression of its target oncogenes by creating large deposits of active histone marks exclusively at enhancers, collaboratively with myogenic TFs, and by recruiting chromatin reader bromodomain-containing protein 4 (BRD4), which function at looped enhancer–promoter pairs within topological domain boundaries. Integrating epigenetic and mechanistic drug screening data exposed multiple biological nodes of chemical vulnerability, including BET bromodomains. The BRD4 inhibitor JQ1 has recently shown efficacy in RMS (13), but no mechanistic connection has been shown between BRD4 and PAX3–FOXO1. Here, we report that BRD4 inhibition disrupts a hitherto undiscovered PAX3–FOXO1 interaction with BRD4, causes a rapid degradation of the fusion gene, and ablates its transcriptional output, thus revealing a subtype-selective therapeutic vulnerability to BRD4 inhibition.

[1]Genetics Branch, NCI, NIH, Bethesda, Maryland. [2]Pediatric Oncology Branch, Center for Cancer Research, NCI, NIH, Bethesda, Maryland. [3]Division of Preclinical Innovation, National Center for Advancing Translational Sciences, NIH, Rockville, Maryland. [4]University Children's Hospital, Zurich, Switzerland. [5]Department of Oncohematology, Ospedale Pediatrico Bambino Gesù Research Institute, Rome, Italy. [6]Laboratory of Pathology, NCI, NIH, Bethesda, Maryland. [7]Laboratory of Proteomics and Analytical Technologies, Advanced Technologies Center, NCI, Frederick, Maryland. [8]Systems Biology Center, National Heart, Lung, and Blood Institute, NIH, Bethesda, Maryland.

**Note:** Supplementary data for this article are available at Cancer Discovery Online (http://cancerdiscovery.aacrjournals.org/).

**Corresponding Author:** Javed Khan, NIH, 37 Convent Drive, Building 37, Room 2016B, Bethesda, MD 20892. Phone: 240-760-6135; Fax: 301-480-0314; E-mail: khanjav@mail.nih.gov

**doi:** 10.1158/2159-8290.CD-16-1297

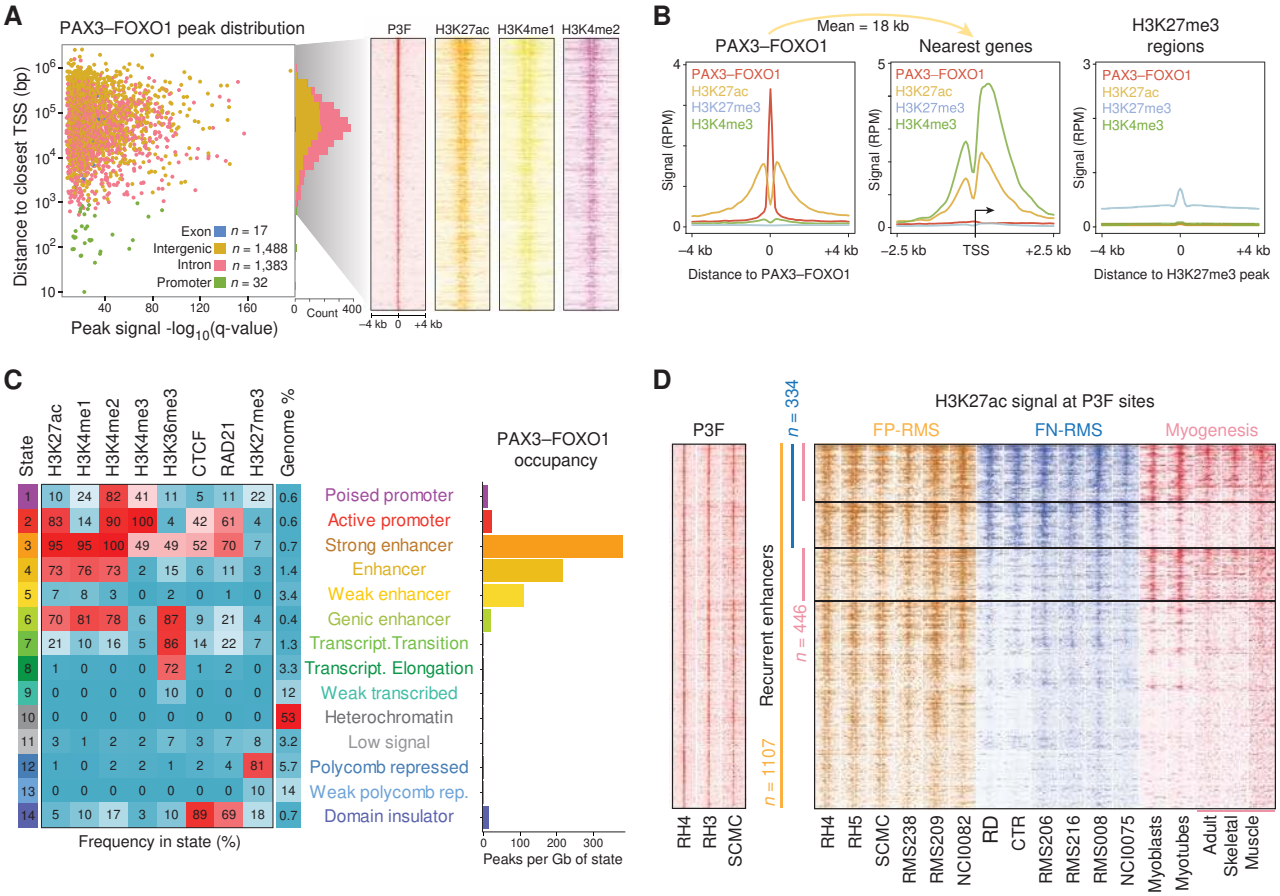


**Figure 1.** Chromatin state mapping pinpoints PAX3-FOXO1 (P3F) in active enhancers. **A,** PAX3-FOXO1 peak distribution and heat maps of PAX3-FOXO1, H3K27ac, H3K4me1, and H3K4me2 at distal regulatory elements in PAX3-FOXO1-bearing cell line (RH4). The scatter plot is accompanied by a histogram showing the amounts of PAX3-FOXO1 in intronic, exonic, intergenic, or promoter-proximal sites. TSS, transcription start site. Rows are centered around PAX3-FOXO1 peaks and extended 4 kb in each direction, sorted by PAX3-FOXO1 signal strength. **B,** PAX3-FOXO1, H3K27ac, H3K27me3, and H3K4me3 signal at PAX3-FOXO1 peaks (left), genes nearest to PAX3-FOXO1 peaks (center), and Polycomb-repressed chromatin (right). Mean distance of PAX3-FOXO1 to its nearest genes (18 kb) is indicated. **C,** Chromatin states in FP-RMS cells (left) and abundance of PAX3-FOXO1 peaks per Gb of each state (right). States were discovered *de novo* using ChIP-seq data for all histone marks (plus, CTCF and RAD21) with the hidden Markov modeling algorithm chromHMM, which bins the genome into states by recurring patterns. Frequency corresponds to the probability of each mark being present in a given state. **D,** High-confidence PAX3-FOXO1 sites bound to enhancers recurrent ($n = 1,107$) in FP-RMS cell lines and tumors, some of which are shared with FN-RMS ($n = 334$) and/or myogenic cells and tissue ($n = 446$).

## RESULTS

### PAX3–FOXO1 Establishes Active Chromatin at Distal Enhancers

The hallmark reciprocal translocation of chromosomes 2 and 13 (14) has coding potential for two fusion proteins (Supplementary Fig. S1A), but the only expressed allele has the 5′ end of PAX3 (DNA binding domain) and the 3′ transactivation domain of FOXO1 (Supplementary Fig. S1B). To gain insight into the epigenetic consequences of PAX3–FOXO1, we mapped the landscape of active and repressive histone marks by sequencing DNA enriched by chromatin immunoprecipitation (ChIP-seq) from a patient-derived fusion-positive FP-RMS cell line, RH4. Genome-wide, PAX3–FOXO1 resided predominantly (99%) in sites more than 2.5 kb distal from the nearest transcriptional start site (15), all of which harbored active enhancer marks (Fig. 1A), including acetylation at histone 3 lysine 27 (H3K27ac) and H3 lysine 4 mono/dimethylation (H3K4me1 and H3K4me2), but not the active promoter-associated mark H3K4me3 (Fig. 1B). PAX3–FOXO1 sites showed no evidence of poised and repressed chromatin, as demarcated by Polycomb-deposited trimethylation of H3 lysine 27 (H3K27me3), and, conversely, regions marked by H3K27me3 lacked both PAX3–FOXO1 and H3K27ac (Fig. 1B). Because histone marks are deposited in a combinatorial fashion, we defined reoccurring patterns associated with various chromatin functional states (16), providing the first epigenomic map upon which to overlay PAX3–FOXO1 occupancy (Fig. 1C). We found PAX3–FOXO1 most frequently occupied the strong enhancer chromatin state (Fig. 1C), exemplified by known PAX3–FOXO1 target *FGFR4* (Supplementary Fig. S1C) and oncogenes *MYC, ALK,* and *MET* (Supplementary Fig. S1D).

## Binding of PAX3–FOXO1 to Enhancers of High Disease and Biological Relevance

To identify which of these PAX3–FOXO1 sites are of high disease relevance, we first performed ChIP-seq in two additional cell FP-RMS lines, RH3 and SCMC, to identify a broader set of targets and recurrent sites. There were 1,783 peaks shared among 2 and 555 peaks for all 3 cell lines, and these showed the most statistical significance and largest signal per peak (Supplementary Fig. S1E–S1F). We next mapped a key histone marker of enhancers H3K27ac in a panel of FP-RMS cell lines and tumor samples, and found 1,107 high-confidence PAX3–FOXO1 sites occupying enhancers in one or more of the cell lines (Fig. 1D; Supplementary Table S1). We then generated a similar map of enhancers in FN-RMS cell lines and tumors, which shared 334 enhancer loci. Four hundred forty-six PAX3–FOXO1-bound enhancers were also present in myogenic samples. The enhancers unique to FP-RMS were enriched, by GREAT ontology (17), in pathways involved in early development, whereas shared enhancers were enriched for late muscle differentiation (Supplementary Fig. S1G).

PAX3–FOXO1 acting across large one-dimensional sequence distances has confounded target gene identification. Previous reports to identify these targets were based on either changes in gene expression (11, 12, 18) or proximity of a gene to a PAX3–FOXO1 peak in a single-cell line with no consideration of expression or chromatin context (15). We therefore identified high-confidence PAX3–FOXO1 target genes by a series of criteria (see Supplementary Fig. S2A–S2B and Supplementary Methods). In brief, we (i) used only PAX3–FOXO1 bound to enhancers that were recurrent in cell lines and tumors (from Fig. 1D), (ii) selected for expressed genes, as PAX3–FOXO1 was found only in active chromatin states, (iii) excluded nearby expressed genes if they were not found within the same topologically associated domain (TAD; predicted by HiC data, ref. 19) as the PAX3–FOXO1 bound enhancer, and (iv) included the maximally expressed gene within each TAD harboring PAX3–FOXO1. Using this approach, we found 1,010 high-confidence targets, 678 of which were novel, and, of note, 439 were significantly reduced by short hairpin RNA (shRNA) knockdown of PAX3–FOXO1 for 48 hours (Supplementary Fig. S2C–S2G). Novel targets included oncogenes ($n = 24$), TFs ($n = 53$), and several imprinted genes ($n = 7$; Supplementary Table S2).

Thus, our data support the hypothesis that PAX3–FOXO1 enables transcription by directing active chromatin marks to distal enhancers surrounding oncogenes, imprinted and myogenic genes.

## FP-RMS Tumors and Cell Lines Possess a Myogenic Transcriptional Program

TFs act on enhancers in a stoichiometric manner, and those that are expressed at unusually high concentrations and are able to bind a majority of enhancers are defined as master transcription factors (MTF) and key determinants of cell fate (1). Although PAX3–FOXO1 is the primary driver, as an MTF it is likely to not work alone. We identified other MTFs that were overexpressed compared with normal tissues ($P < 10^{-30}$), had consistently high levels (average FPKM >20), were super enhancer regulated, and had significant motif enrichment in enhancers (Fig. 2A). To do this, we first compared the RNA-sequencing (RNA-seq) profiles of RMS primary tumors

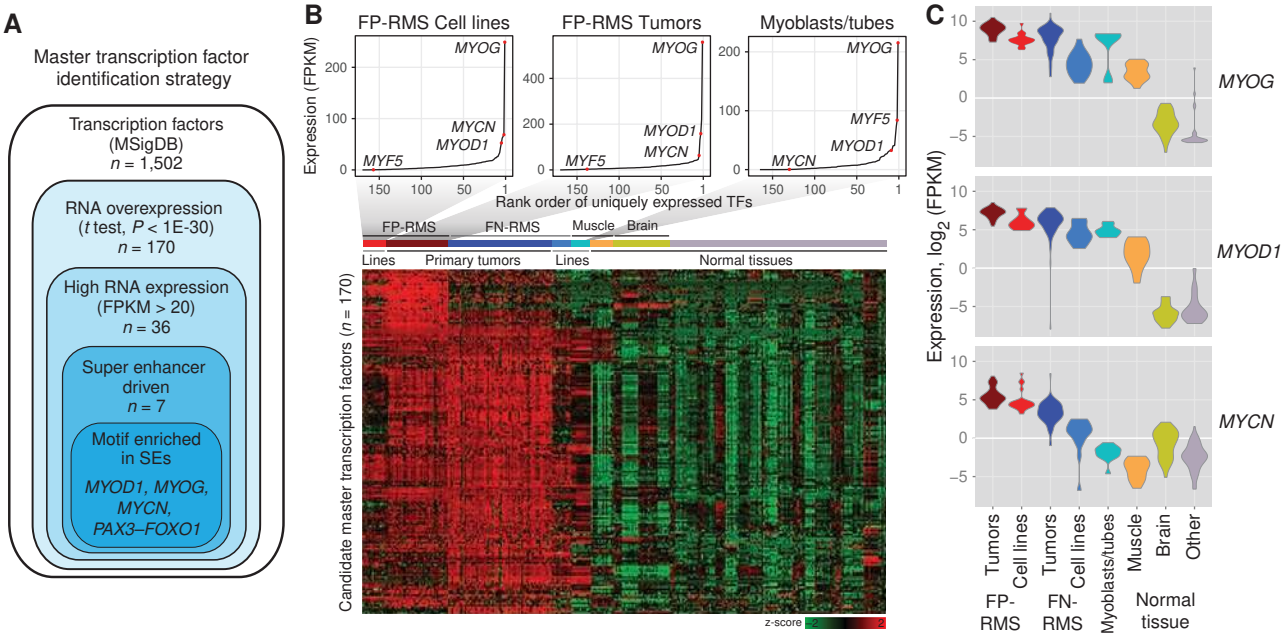


**Figure 2.** Transcriptional and epigenetic landscapes of RMS cell lines and primary tumors. **A,** Strategy for identifying MTFs from RNA-seq and ChIP-seq datasets. **B,** RNA sequencing of patient RMS tumors reveals a set of candidate MTFs ($n = 170$) identified by filtering for significant overexpression ($P < 1E-30$) across one or both RMS subtypes, and removal of general TFs (those ubiquitously expressed in all tumors and tissues). Candidates were ranked and plotted based on average overall expression in fusion-positive RMS (cell lines and tissues) and myoblasts/myotubes. **C,** Violin plots of gene expression of *MYOD1*, *MYOG*, and *MYCN* across RMS, myoblasts, myotubes, and normal tissues. (*continued on next page*)

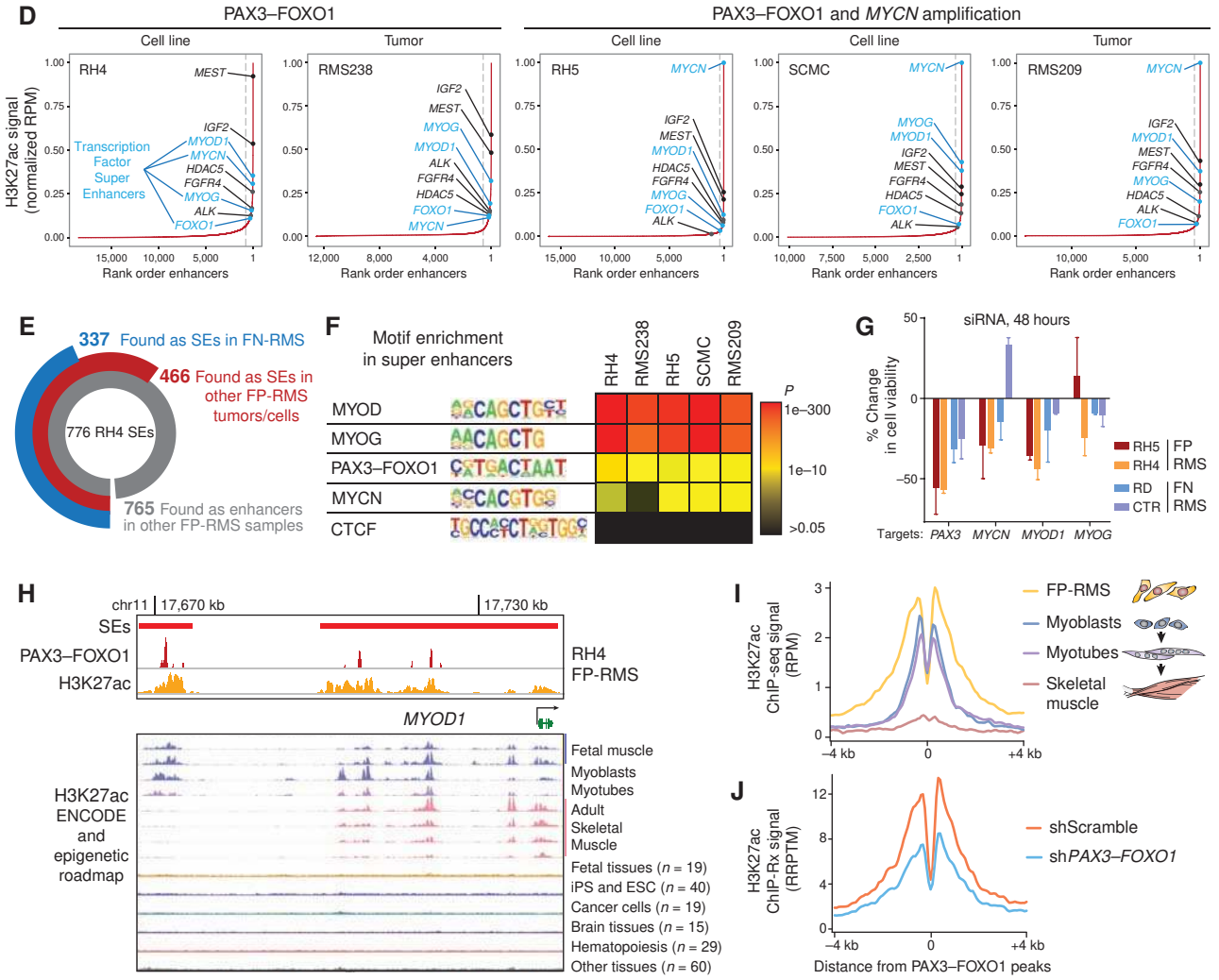


**Figure 2.** (***Continued***) **D,** H3K27ac binding at distal enhancers ranked by increasing signal in cell lines and primary tumors bearing PAX3–FOXO1 translocation. Super enhancers (SE) were identified as those beyond the inflection point where rapid increase in signal is observed (indicated by a dashed gray line). TF genes associated with SEs are indicated in blue. **E,** Number of RH4 SEs which occur as enhancers ($n = 765$) and SEs in FP-RMS cell lines or tumors ($n = 466$), or which also appear in FN-RMS as SEs ($n = 337$). **F,** Enrichment of known recognition sequences for MYOD, MYOG, PAX3–FOXO1, and MYCN, compared with no enrichment for CTCF in FP-RMS SEs. **G,** Reduction in cell viability upon siRNA against PAX3, MYOD1, MYOG, and MYCN in FN-RMS (RD, CTR) and FP-RMS (RH4, RH5) cells. *PAX3* siRNAs targeted the first few exons, which are intact in the fusion PAX3–FOXO1. CellTiter-Glo was used to measure viability, and all data were normalized to cells treated with scrambled siRNA. Bars show median (error bars = range) of 3 independent siRNA sequences (RH5, RD, and CTR) or 2 independent sequences (RH4). Experiments were performed at 48 hours of transient siRNA transfection. **H**, *MYOD1* enhancers are bound by PAX3–FOXO1 and loaded with active histone mark H3K27ac in RH4 cells (top) and are progressed through myogenesis (middle) and are absent in other cell and tissue types (overlapping plots, bottom). ENCODE and Epigenome Roadmap data tracks are provided at WashU Epigenome browser session http://epigenomegateway.wustl.edu/browser/?genome=hg19&session=IHfj0MDWoA&statusId=728028850. iPS, induced pluripotent stem cells; ESC, embryonic stem cells. **I,** Myogenic enhancers at PAX3–FOXO1 binding sites diminish through muscle differentiation. RPM, reads per million mapped reads. FP-RMS signal is from RH4 cells, myoblasts, and myotubes are from ENCODE; skeletal muscle data are from a normal tissue sample. **J**, Same enhancer locations as **I** interrogated for H3K27ac signal in RH4 cells treated with shRNA for 48 hours (shScramble or sh*PAX3–FOXO1*). Signal was normalized to spike-in *Drosophila* reads (ChIP with reference exogenous genome, ChIP-Rx) and are plotted as reference adjusted reads per 10 million (RRPTM).

($n = 103$) and cell lines ($n = 37$; ref. 3) with normal human organ tissues ($n = 188$). This identified a consistently overexpressed core of 170 TFs, suggesting a convergent underlying epigenetic state (Fig. 2B; Supplementary Table S3). The TFs, of these RMS tumors resembled those of myoblasts and myotubes (20), and all have remarkably high levels of the lineage-determining TFs *MYOD1* and *MYOG* as compared with other normal tissues (Fig. 2B and C). Unlike myoblasts, *MYF5* is typically missing from RMS, although when present it appears to be mutually exclusive with *MYOD1* (21). Another important divergence from normal myogenesis was high expression of the transcriptional amplifier *MYCN* (Fig. 2C), a known target of PAX3–FOXO1 (15). *MYCN* expression was generally higher in FP-RMS tumors whereas *MYC* expression was higher in FN-RMS; however, many tumors had expression of both, such that the sum was consistently high for all

patients with RMS (Supplementary Fig. S3A and S3B). RMS cell lines faithfully recapitulated the transcriptional commitment of the primary tumors to these candidate MTFs.

## Super Enhancer Analysis in RMS Cell Lines and Primary Tumors Implicates MYOD, MYOG, and MYCN as Master Regulators

A small fraction of active enhancers acquire a large fraction of transcriptional machinery and active chromatin marks (frequently demarcated by H3K27ac), and have been defined as super enhancers (22, 23). These regions are cell type–specific and control expression of cell identity genes in normal tissues and oncogenes in cancer. Although super enhancers may simply be clusters of additive enhancers (24), they nevertheless capture the most active enhancers associated with the core regulatory MTF circuitry (25). In RMS cells bearing PAX3–FOXO1 (RH4), we identified 776 super enhancers (ranked as the top 4% of all enhancers with 38% of the total H3K27ac signal) that were associated with hallmark RMS genes such as *IGF2, FGFR4, ALK, MYOD1, MYOG*, and *MYCN* (Fig. 2D). To evaluate the clinical relevance of our cell lines as models for enhancer architecture, we mapped super enhancers by H3K27ac signal in a set of 3 FP-RMS and 5 FN-RMS primary tumors. We found concordance of super enhancers among PAX3–FOXO1-driven cell lines and tumors (Fig. 2D). *MYCN* had the highest ranked super enhancer in *MYCN*-amplified cell lines and tumors. A common epigenetic landscape was found in FN-RMS cell lines and tumors (Fig. 2E; Supplementary Fig. S3C), which differed from FP-RMS at super enhancers such as *FOXO1, MYCN,* and *ALK* (Supplementary Fig. S3D). *MYCN* itself possessed a remarkable 5 super enhancers within the surrounding TAD structure (HiC data from ref. 19), which circularized chromatin conformation capture followed by sequencing (4C-seq) revealed all physically interact not only with *MYCN*, but also with each other (Supplementary Fig. S3E). Motif analysis at super enhancer sites revealed a highly significant enrichment of MYOD, MYOG, PAX3–FOXO1, and MYCN recognition sequences (Fig. 2F; Supplementary Table S4). Importantly, we observed a consistent reduction in cell viability in 2 FP-RMS cell lines when *PAX3, MYCN,* or *MYOD1* were targeted by siRNAs (Fig. 2G). The suppression was greater in FP-RMS than in FN-RMS, further implicating them as essential master regulators of FP-RMS.

MYOD alone can reprogram cells into myogenesis (26), and it is intriguing that FP-RMS tumors remain undifferentiated despite extremely high levels of the myogenic TFs MYOD and MYOG. Given this, we hypothesized that PAX3–FOXO1 acts as a strong chromatin activator, preventing decommissioning of distal enhancers that are lost during normal muscle differentiation. To study this, we analyzed active enhancer mark H3K27ac (27) around PAX3–FOXO1 peaks, in myoblasts, myotubes, and muscle tissue. We found that enhancers controlling *MYOD1* decreased during muscle differentiation and were absent in other tissues and cell lines, whereas in FP-RMS cells the *MYOD1* enhancer locus was expanded and contained multiple PAX3–FOXO1 peaks (Fig. 2H). Genome-wide, myogenic enhancers found at PAX3–FOXO1 peaks decreased during the transition from myoblasts to myotubes to skeletal muscle (Fig. 2I). Genes associated with these decommissioned enhancers included TFs (*MYCN, MYC, MSC,* and *MYOD1* itself) and epigenetic modulators which have known involvement in regulating self-renewal, embryonic development, muscle development, and chromatin organization (Supplementary Table S5), and imprinted genes involved in mesoderm development (*MEST, IGF2*). These data suggest that PAX3–FOXO1 may induce a myoblastic state by maintaining active chromatin at enhancers controlling these genes. This was further supported by the observation that after 48 hours of PAX3–FOXO1 knockdown these enhancers lost substantial H3K27ac signal as measured by ChIP with reference exogenous genome (ChIP-Rx; ref. 28; Fig. 2J).

## PAX3–FOXO1 Collaborates with MYOG, MYOD, and MYCN at Super Enhancers

Our results indicated that PAX3–FOXO1 activates the MTFs MYOD, MYOG, and MYCN, and together with these, establishes the epigenome and transcriptome of FP-RMS (Fig. 3A). To validate this, we performed ChIP-seq on MYOD, MYOG, and MYCN and studied the extent of their collaboration with PAX3–FOXO1 to shape the enhancer landscape. We observed widespread binding of MYOD, MYOG, and MYCN, each covering 9 to 15 times as much genomic space as PAX3–FOXO1 (Supplementary Fig. S4A). When all four MTFs were colocalized in the genome they harbored greater signal of active histone marks, especially H3K27ac (Supplementary Fig. S4B–S4C). Enhancers with all 4 MTFs were frequently super enhancers (Fig. 3B). Almost every super enhancer was occupied by 3 or more of these MTFs, unlike typical enhancers (Fig. 3C). Super enhancers spanned a median of 23.5 kb (compared with 1.2 kb for typical enhancers) and exhibited a higher load of MTFs only when considering their constituent peaks (Fig. 3C; Supplementary Fig. S4D). PAX3–FOXO1 occupied only a small fraction of typical enhancers (5%) but many super enhancers (47%). MYOG, MYOD, and MYCN are bound to almost every super enhancer, and although PAX3–FOXO1 was found in only half of all super enhancers, its preference for super enhancers over typical enhancers was profound (Fig. 3D and E). Super enhancer–associated genes were transcribed at significantly higher levels than typical enhancer genes, and enhancers occupied by 4 MTFs were found to be most highly transcribed compared with enhancers with fewer MTFs (Fig. 3F).

The genome-wide placement of super enhancers was strongly determined by the myogenic MTFs recognizing the underlying DNA sequence CAGCTG (Fig. 2F), but interestingly there was low enrichment of the canonical MYCN motif CACGTG (Supplementary Table S4). More than 80% of MYCN peaks were distal (Supplementary Fig. S4E), and *de novo* motif analysis discovered MYCN prefers a myogenic E-box sequence (RRCAGCTG) nearly identical to that of MYOG and MYOD (Supplementary Fig. S4F). Thus, MYCN may behave in a manner akin to MYC acting as a general transcriptional amplifier, following to locations opened by more sequence-specific (and lineage determining) TFs (29, 30).

Master (or lineage determining) TFs are predicted to maintain cell identity by mutual and self-reinforcement, creating autoregulatory feed-forward loops (1, 31). We found this to be the case in FP-RMS, where the super enhancers controlling *PAX3–FOXO1, MYOD,* and *MYCN* contain all four of these MTFs (Fig. 3G). The *MYOG* super enhancer is bound by all except the PAX fusion, consistent with the logic and timing of normal

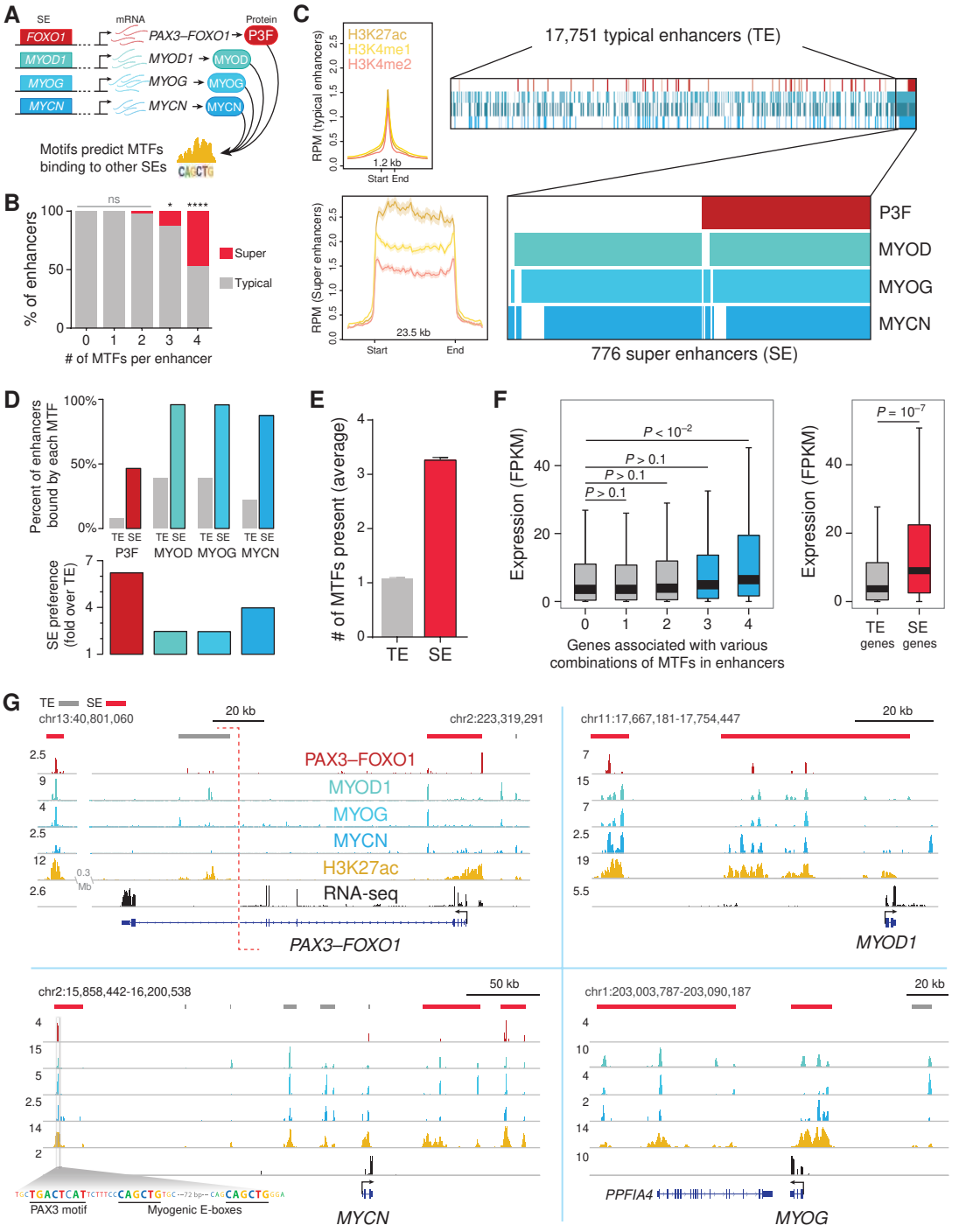


**Figure 3.** PAX3–FOXO1 (P3F) collaborates with MTFs MYOD, MYOG, and MYCN at super enhancers (SE). **A,** Characteristics enlisting candidate MTFs in FP-RMS: SE-driven, high expression, with motifs enriched across all SEs predicting TF binding. **B,** The percentage of enhancers (divided into groups by the number of MTFs therein) which classify as either typical (TE) or super. Null hypothesis (that the % of super enhancers does not depend on number of MTFs present in an enhancer) was evaluated with Fisher exact test; *, $P < 0.04$; ****, $P < 0.0001$; ns, not significant. **C,** Left, read density profiles of H3K27ac, H3K4me1, and H3K4me2 at regions of TE and SE architecture. Median enhancer length is indicated. Right, collaborative co-occupancy of MTFs in TEs and SEs. Presence of each MTF at enhancer is indicated by the respective colors. **D,** Top, enhancer occupancy of each MTF at TEs or SEs. Bottom, fold enrichment of SEs over TE for each MTFs. **E,** Average number of MTFs per enhancer type. Error bars show 95% confidence interval. **F,** Expression of genes associated with enhancers of various MTF combinations (left) or SE and TE genes (right), associated by proximity. RNA-seq reported as FPKM, fragments per kilobase of transcript per million mapped reads. Error bars, 95% confidence interval. *P* values calculated by Welch unpaired *t* test. **G,** Mutual and self-reinforcement of MTFs via SEs for *PAX3–FOXO1*, *MYOD1*, *MYCN*, and *MYOG*. Tracks show signal in RPM, reads per million mapped reads. TEs are indicated by gray bars and SEs by red. To illustrate an example of multiple adjacent motifs presence within SEs, we have zoomed in on the PAX3 and MYOD/MYOG motifs present upstream of *MYCN*.

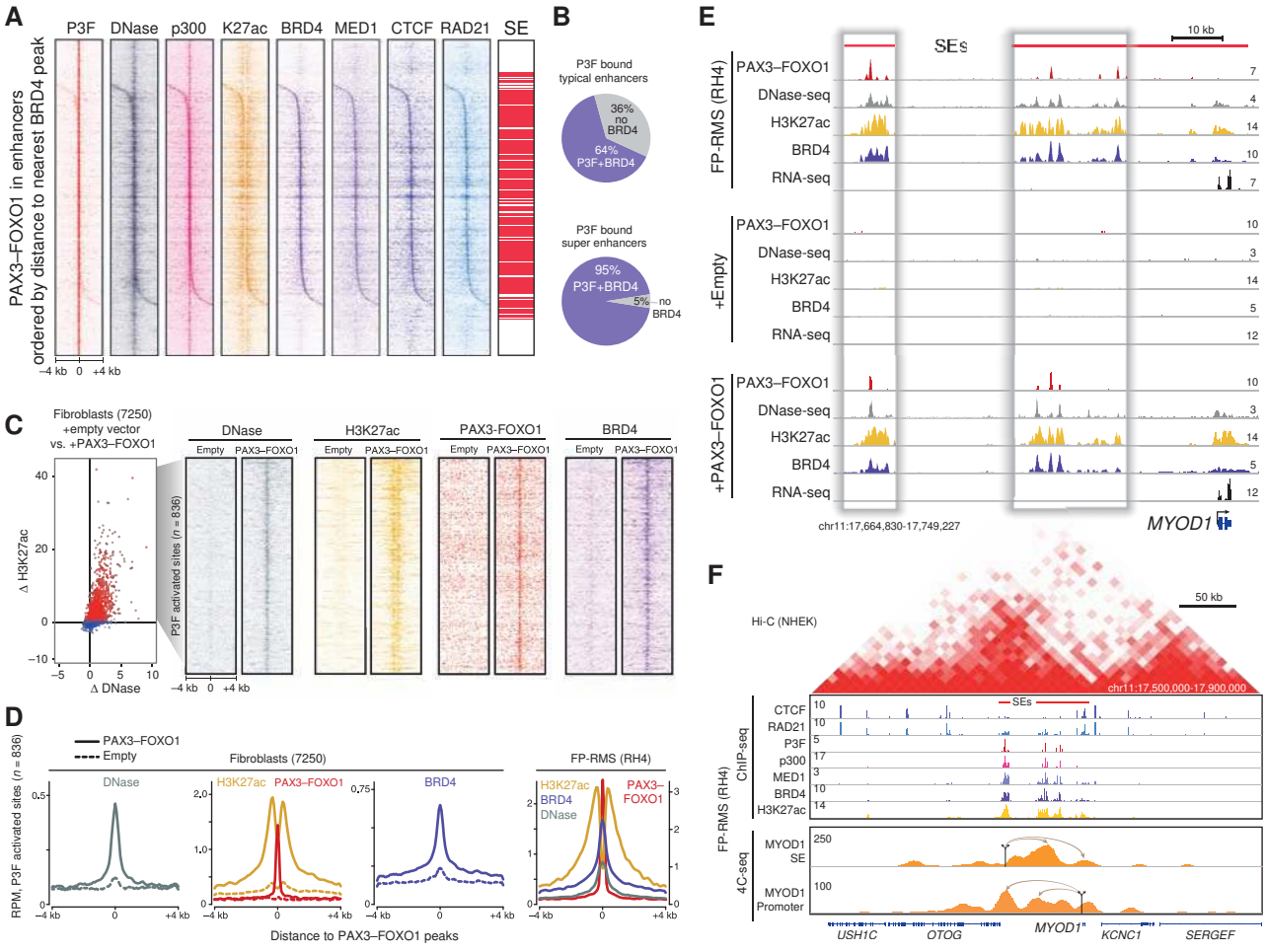


**Figure 4.** PAX3–FOXO1 (P3F) opens chromatin and recruits BRD4 at looped enhancers. **A,** Heat maps of PAX3–FOXO1, DNase, p300, H3K27ac, BRD4, MED1, CTCF, and RAD21 signal at PAX3–FOXO1 peaks, ranked by distance to closest BRD4 peak in RH4. Rug graph indicates which locations (red lines) are within super enhancers (SE). **B,** PAX3–FOXO1 and BRD4 co-occupancy at enhancers (top, typical; bottom, super). **C,** Introduction of PAX3–FOXO1 into a fibroblast causes increased sensitivity to DNase, deposition of H2K27ac and recruitment of BRD4 at PAX3–FOXO1 sites. **D,** Metagene analysis of DNase, H3K27ac, PAX3–FOXO1, and BRD4 upon PAX3–FOXO1 introduction into fibroblasts (left) compared with RH4 cells (end right). **E,** Opening of chromatin at the *MYOD1* SE by PAX3–FOXO1 in fibroblasts (7,250) with empty vector (middle) or PAX3-FOXO1 (bottom), compared with RH4 cells (top). **F,** Hi-C profile (top) surrounding *MYOD1* locus from NHEK cells (19) with CTCF, RAD21, PAX3–FOXO1, p300, MED1, BRD4, and H3K27ac ChIP-seq data in RH4 cells. 4C-seq (bottom) from *MYOD1* SE looping to adjacent SE region and *MYOD1* promoter, and vice versa, in RH4 cells. Viewpoints are indicated by arrows anchored to their genomic locations.

myogenesis which successively progresses from dominance of PAX3 to MYOD to MYOG (32). To investigate the contribution of interconnection to gene expression, we used shRNA against each factor followed by RNA-seq. PAX3–FOXO1 depletion disrupted both enhancer acetylation and RNA expression at *MYOD* and *MYCN*, but an indirect increase at *MYOG* (Supplementary Fig. S4G). *MYOG* expression was the most profoundly reduced by knockdown of either MYOD1 or MYCN (Supplementary Fig. S4H and S4I). All MTFs were sensitive to MYCN depletion, and *MYCN* expression was sensitive to depletion of any one factor (Supplementary Fig. S4G and S4H).

## BRD4, MED1, and p300 Occupy Key PAX3–FOXO1-Established Super Enhancers

Because PAX3–FOXO1 binds between 10Kb and 1Mb away from nearby promoters, it may mediate its transcriptional impact through chromatin factors looping over long distances. The transactivation domain of FOXO1 is known to recruit the coactivator p300 (33), which enzymatically acetylates histones, leading to binding of additional factors, including BRD4 and Mediator (34). We therefore hypothesized that PAX3–FOXO1 recruits p300 and the other cofactors leading to chromatin remodelling. To test this, we performed ChIP-seq of these components and analyzed their co-occupancy at PAX3–FOXO1-bound enhancers. Our results confirmed that these proteins co-occupy enhancers with PAX3–FOXO1 and were sites of open chromatin as determined by DNase hypersensitivity (Fig. 4A). We observed that p300 followed PAX3–FOXO1 at virtually every site, and BRD4 was co-occupant at the majority of these enhancers (72%), especially those with super enhancer architecture (95% of super enhancers; Fig. 4B). PAX3–FOXO1 locations lacking BRD4 showed no evidence of looping machinery MED1, CTCF, and RAD21,

whereas sites bound by BRD4 did (Supplementary Fig. S5A). We predicted that these two PAX3–FOXO1 modes (with and without BRD4; Supplementary Fig. S5B–S5C) would have divergent functional consequences, and found that sites with BRD4 had greatly increased expression from associated genes (Supplementary Fig. S5D), and GREAT ontology analysis showed only BRD4-containing peaks were enriched for FP-RMS gene sets (Supplementary Fig. S5E).

It is unknown if PAX3–FOXO1 itself is capable of inducing *de novo* myogenic enhancer formation. We thus stably expressed PAX3–FOXO1 in a human fibroblast cell line (7250) and studied changes in chromatin and the corresponding changes in gene expression. We found that PAX3–FOXO1 opened the chromatin landscape, as evidenced by an increase in DNA hypersensitivity at enhancers compared with control parental cells (Fig. 4C). Furthermore, PAX3–FOXO1-bound enhancers saw an increase in H3K27ac and recruitment of the acetylated lysine reader BRD4 (Fig. 4C). These sites of opening ($n = 836$) are active, PAX3–FOXO1 bound, and BRD4 loaded in FP-RMS cells (Fig. 4D). Many of the enhancers, such as the super enhancers upstream of *MYOD1* (Fig. 4E), *MYOG,* and *FGFR4* (Supplementary Fig. S5F), are faithfully reconstituted with a size and shape similar to those in RMS. Of the 568 high-confidence PAX3–FOXO1 super enhancers, 349 are recapitulated in these fibroblasts reprogrammed by exogenous PAX3–FOXO1 (Supplementary Fig. S5G).

The proximity of the PAX3–FOXO1-directed super enhancers near *MYOD1* and their coappearance with *MYOD1* transcription led us to predict three-dimensional looping to bring these super enhancers to the promoter. We confirmed these *cis* interactions in RH4, using 4C-seq from two viewpoints (one at the most distal PAX3–FOXO1-bound super enhancer and the other at the *MYOD1* promoter; Fig. 4F). These loops enable the physical interaction of the super enhancer–bound proteins MED1, p300, and BRD4 with the promoter of *MYOD1* to facilitate transcription. The 4C interactions were restrained to the TAD predicted by HiC data (19) in other human cells (Fig. 4F). Thus, PAX3–FOXO1 acts as a pioneering factor, opening chromatin, recruiting coactivators, and driving transcription through looped myogenic super enhancers.

## Molecular Sensitivities of PAX3–FOXO1 Tumor Cells Are Associated with Super Enhancers

Our results thus far showed that PAX3–FOXO1 establishes super enhancers not only at myogenic genes but also at multiple druggable oncogenic drivers. Because super enhancers are cell-type restricted, we hypothesized that FP-RMS would be selectively vulnerable to inhibition of these super enhancer–driven pathways. Hence, we determined the landscape of molecular sensitivities in PAX3–FOXO1-positive patient-derived cell lines (RH41, RH5) by dose responses at 48 hours for 1,912 compounds. To deprioritize compounds with nonselective cytotoxicity, we also treated fibroblast cell lines (NIH3T3, 7250, and T9195). Our small-molecule library MIPE4 (35) was assembled to have high mechanistic diversity with an emphasis on clinically relevant compounds (Supplementary Fig. S6A–S6B; Supplementary Table S6). Area under the dose response curve (AUC) was used as the measure of potency, as this metric captures both dose dependence and maximum response (see Supplemental Methods and Supplementary Fig. S6C–S6E). PAX3–FOXO1-expressing cells were selectively sensitive to super enhancer–driven RTKs (FGFR4, IGF2/IGF1R, and ALK) and downstream kinases (PI3K, AKT, and mTOR). Furthermore, transcriptional cofactors (HDACs, BRD4) originally identified as super enhancer–associated proteins (23) were also selective for FP-RMS cells (Fig. 5A–B; Supplementary Fig. S6F). Thus, the identification of super enhancer–associated genes highlighted multiple candidate targets for therapy, which may be a useful approach for other cancers. Of note, FP-RMS was sensitive to inhibiton of BRD4 (36), which has recently shown promising results in RMS tumor models (13), although no molecular explanation in connection with PAX3–FOXO1 has previously been made. Thus, with these new data reported herein that BRD4 lies at an important node in the PAX3–FOXO1 circuitry (Supplementary Fig. S6G), we next sought a mechanistic explanation for the sensitivity.

## Cells with PAX3–FOXO1 Are Selectively Sensitive to BET Bromodomain Inhibition

Given the sensitivity of FP-RMS cells to chemical BRD inhibition, we sought to determine if this was attributable to PAX3–FOXO1, or if the FN-RMS subtype was also vulnerable. Thus, we tested an expanded panel of RMS cell lines against 5 structurally diverse BET bromodomain inhibitors (BRDi) and 1 pan-bromodomain inhibitor, Bromosporine. Thienodiazepine inhibitors, JQ1 and the clinical analogue OTX015, were the most potent, with dose response consistently in the nanomolar $IC_{50}$ range for FP-RMS cell lines, whereas most often in the micromolar range in fusion-negative (mutant RAS) RMS lines (Fig. 5C; Supplementary Fig. S7A–S7C). BRD4 inhibition dramatically reduced proliferation over time in PAX3–FOXO1-driven cells, whereas mutant RAS-driven RMS cells were relatively unhindered (Fig. 5D; Supplementary Fig. S7D). JQ1 action was mediated by programmed cell death in a dose-dependent manner (Supplementary Fig. S7E). Importantly, although *MYCN* amplification clearly confers special sensitivity to BRD4 inhibition in neuroblastoma (37), FP-RMS cells with (RH5 and SCMC) or without (RH3, RH4, and RH41) *MYCN* amplification were all sensitive (Fig. 5C). PAX3–FOXO1 also conferred 11-fold increased BRDi sensitivity to fibroblasts (Fig. 5E). Patient-derived xenografts grown in culture further confirmed PAX-fusion vulnerability, and FN-RMS resistance, to JQ1 (Supplementary Fig. S7F).

The JQ1 targets BRD2/3/4 (but not BRDT) are expressed in RMS, but not overexpressed compared with normal tissues (Supplementary Fig. S8A). RNAi screening of bromodomain-containing proteins revealed greatest dependence on *EP300, KAT2A, BRD3,* and *BRD4* (Supplementary Fig. S8B). Among the BET family members, *BRD4* was the most sensitive to genetic depletion, which incurred apoptotic events (Supplementary Fig. S8C–S8E).

## PAX3–FOXO1 Requires BRD4 for Function and Stability

The sensitivity of PAX3–FOXO1-driven cell lines to BET inhibition and our data showing co-occupancy of BRD4 in all PAX3–FOXO1-bound super enhancers led us to the hypothesis that PAX3–FOXO1 is dependent on BRD4 to mediate transcription of its target genes. This is consistent with the known role of BRD4 in stimulating transcriptional elongation (38) and previous reports that BRD4 inhibition causes rapid

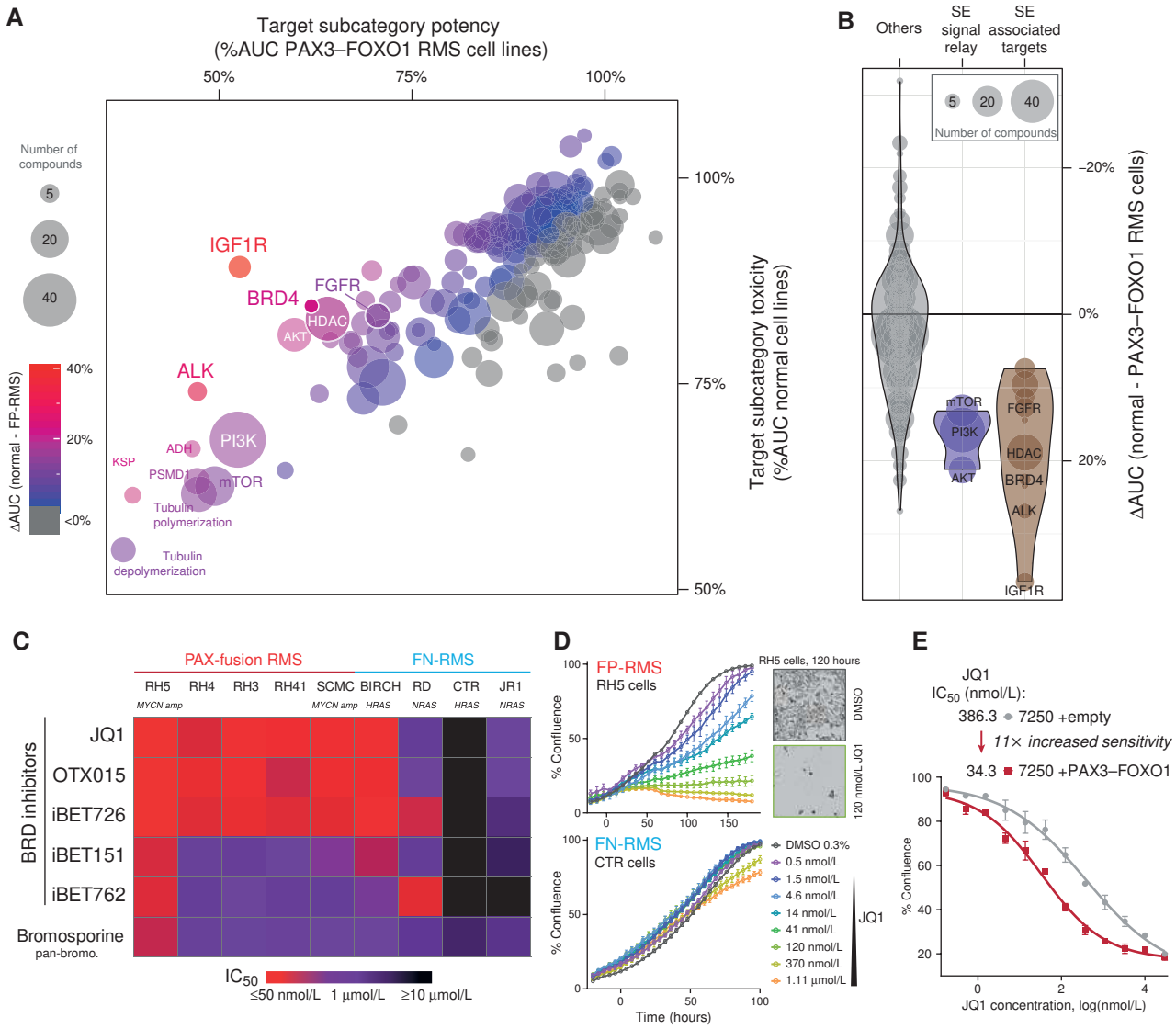


**Figure 5.** Molecular sensitivity landscape of FP-RMS is enriched in super enhancer (SE)–associated targets including BRD4. **A,** Potency in PAX3–FOXO1 RMS cell lines versus toxicity in normal cell lines measured by dose response and summarized across 240 mechanistically distinct subcategories. The percent area under the dose response curve (%AUC) was averaged for all compounds within a target subcategory. The number of compounds in each category is indicated by the size of the bubble, and the difference in AUC (normal – RMS) is indicated by color scale. **B,** Differential sensitivities against molecules targeting proteins associated with SEs, compared to non-SE targets and SE-signal transduction. Size of the bubble indicates number of molecules against each target. **C,** $IC_{50}$ heat map of 5 BET bromodomain inhibitors and 1 pan-bromodomain inhibitor across 5 PAX-fusion and 4 fusion-negative RMS cell lines. **D,** Growth curves of FP-RMS cells (RH5) and FN-RMS cells (CTR) exposed to increasing concentrations of JQ1 or DMSO. Confluence measured by phase-contrast images every 4 hours over multiple days of treatment. Inset, images of RH5 cells with DMSO or 120 nmol/L JQ1. **E,** PAX3–FOXO1 increases sensitivity of fibroblasts to JQ1.

decommissioning of super enhancers and selective inhibition of super enhancer–driven genes (39). To test this, we compared the fold change in super enhancer–associated versus typical enhancer–associated genes before and after treatment with JQ1 for 6 hours by RNA-seq. Indeed, we found that super enhancer–associated genes in FP-RMS cells were especially sensitive to JQ1, and that this selectivity was also seen upon genetic depletion of PAX3–FOXO1 itself (Fig. 6A; Supplementary Table S7). Gene set enrichment analysis (GSEA) revealed that JQ1 was able to selectively downregulate PAX3–FOXO1 target genes, with enrichment mirroring knockdown of PAX3–FOXO1 (Fig. 6B; Supplementary Fig. S9A–S9B). Many key super enhancer–driven TFs and PAX3–FOXO1 targets were suppressed whereas cell-cycle arrest and apoptosis genes were upregulated by JQ1 (Fig. 6C). The known sensitivity of MYC family proteins to BRD inhibition was seen at both the transcript and protein levels (Fig. 6C; Supplementary Fig. S9C). Coordinately, master regulators MYOD and MYOG were also reduced at the protein level upon JQ1 treatment in a dose- and time-dependent fashion (Fig. 6D; Supplementary Fig. S9D). These effects were not a consequence of reducing PAX3–FOXO1 transcription, as evidenced by exon-level expression in RNA-seq data (Fig. 6E).

Although ChIP-seq evidenced that BRD4 and PAX3–FOXO1 are co-occupant spatially, it was unclear whether they bind

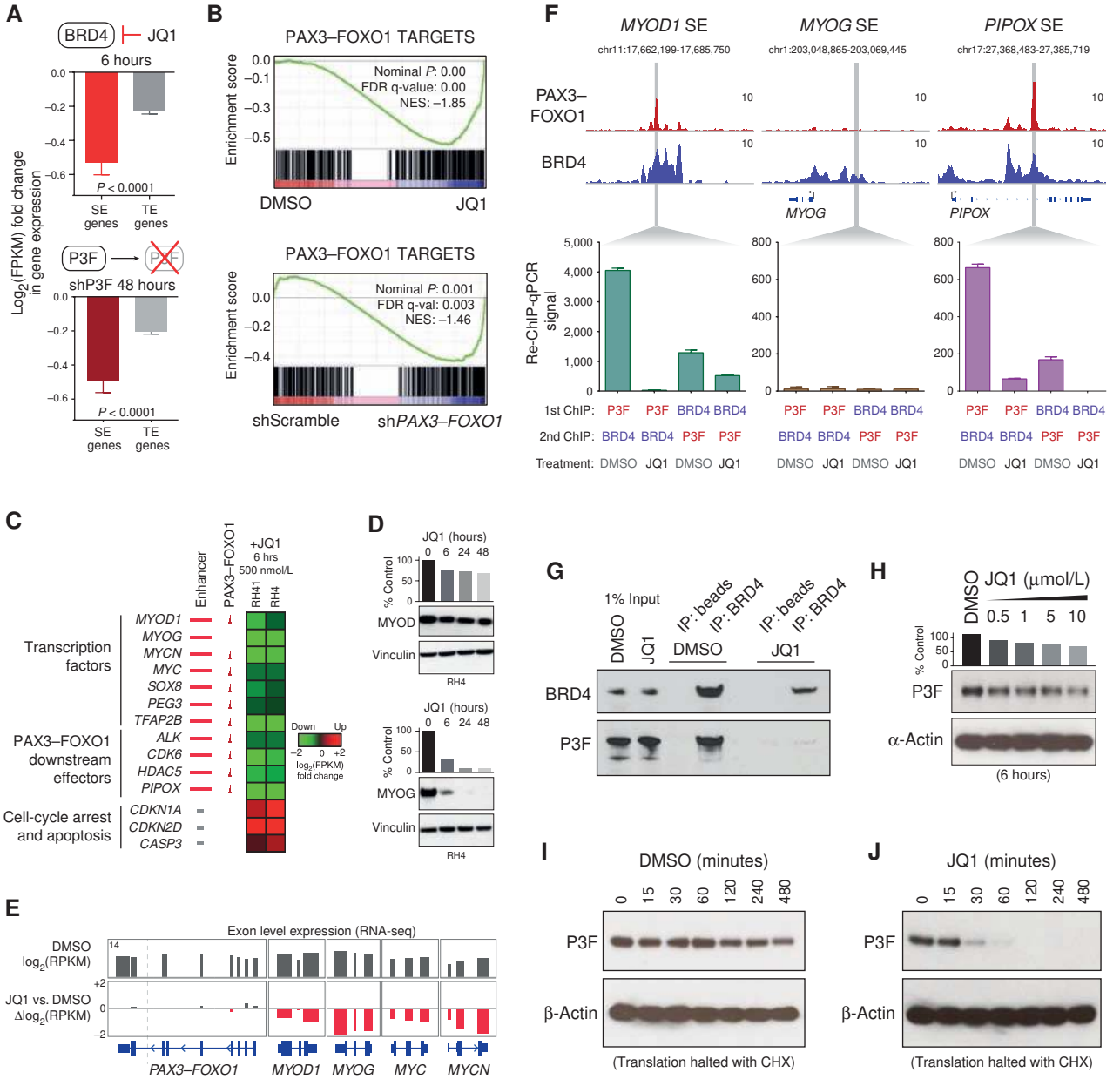


**Figure 6.** JQ1 selectively ablates PAX3–FOXO1-driven transcription and BRD4 interaction. **A,** Selective disruption of super enhancer (SE) genes upon BET bromodomain inhibition (top) or inducible shRNA depletion of PAX3–FOXO1 (P3F; bottom) in RMS cells (RH4). Fold change in gene expression calculated by comparison with log2 of FPKM in controls (DMSO, scramble shRNA). Error bars show the 95% confidence interval. *P* values calculated by Welch's unpaired *t* test. **B,** GSEA revealed the inhibition of PAX3–FOXO1 fusion gene targets, both by JQ1 and PAX3–FOXO1 knock down. NES, normalized enrichment score; FDR, false discovery rate. Genes used were high-confidence PAX3–FOXO1 targets with recurrent enhancers in 83–100% of FP-RMS samples, as reported in Supplementary Table S2. **C,** mRNA expression alterations of SE (red bar) and PAX3–FOXO1 (red peak) targets after 6 hours of 500 nmol/L JQ1 treatment in RH41 and RH4 cells. Heat map indicates the $\log_2$ fold change in FPKM. **D,** Protein levels of MYOD and MYOG by immunoblotting of RH4 cell lysates after treatment with JQ1(1 μmol/L) over time. **E,** Exon level expression and fold change in RH4 cells upon JQ1 treatment (6 hours, 500 nmol/L), for *PAX3–FOXO1, MYOD1, MYOG, MYC,* and *MYCN*. *PAX3–FOXO1* expression remains intact upon JQ1 treatment, unlike the other key TFs. **F,** BRD4 and PAX3–FOXO1 localization shown via ChIP-seq (top) and re-ChIP-qPCR in the presence and absence of JQ1 (bottom) at the *MYOD* upstream SE, *MYOG* downstream SE and *PIPOX* intronic SE. RH4 cells were treated for 6 hours with DMSO or 1 μmol/L JQ1. **G,** Coimmunoprecipitation of PAX3–FOXO1 and *BRD4* from RH4 cells treated with DMSO or 1 μmol/L JQ1 for 24 hours. **H,** PAX3–FOXO1 immunoblot after 6-hour treatment of DMSO or JQ1 with increasing concentrations. Bar chart (top) quantization of PAX3–FOXO1 normalized to loading controls (β-actin). **I–J**, Stability of PAX3–FOXO1 protein measured by immunoblotting after halting translation with cycloheximide (CHX) in RH4 cells treated with DMSO or JQ1 (1 μmol/L).

chromatin cotemporally. To study this, we performed tandem chromatin immunoprecipitations (re-ChIP) for PAX3–FOXO1 followed by BRD4, and vice versa, in RH4 cells treated with either DMSO or JQ1 for 6 hours. Quantitative PCR of re-ChIP DNA at enhancer sites bound by both PAX3–FOXO1 and BRD4 (*MYOD1, PIPOX*) revealed strong enrichment regardless of ChIP order (Fig. 6F), which was almost completely ablated in JQ1-treated cells. This was not observed at BRD4-only enhancers near *MYOG*. To corroborate this, we performed coimmunoprecipitation with BRD4 and PAX3–FOXO1 in the presence of DMSO or JQ1 (Fig. 6G), and found that JQ1 indeed ablated this endogenous interaction. The PAX3–FOXO1 and BRD4 interaction was seen in both directions using exogenous, tagged versions of these proteins (Supplementary Fig. S9E). Given no alteration in *PAX3–FOXO1* mRNA levels, and only modest reduction in protein levels (Fig. 6H), we suspected JQ1 caused destabilization of the PAX3–FOXO1 protein. Remarkably, the half-life of PAX3–FOXO1 was reduced from >8 hours to 28 minutes with JQ1 compared to DMSO (Fig. 6I–J; Supplementary Fig. S9F) in the presence of cycloheximide to inhibit protein translation. This appears to be an on-target effect, as shRNA against BRD4 also caused PAX3–FOXO1 to decrease at the protein level, but not the transcript level (Supplementary Fig. S9G). Thus, PAX3–FOXO1 interacts with BRD4 at enhancers, and treatment with JQ1 leads to loss of this interaction with rapid degradation of PAX3–FOXO1 protein.

### JQ1 Selectively Disrupts PAX3–FOXO1-Driven Transcription to Suppress Tumor Growth *In Vivo*

The *in vitro* sensitivity of FP-RMS to BRD4 inhibition by the rapid and the specific inhibition of PAX3–FOXO1 function indicated this may be an effective therapeutic strategy. To test this, we developed an imagable readout to monitor *in vivo* activity of PAX3–FOXO1 super enhancer affected by drugs administered to mice. We engineered RMS cells to express luciferase (and GFP), controlled either by a constitutively active cytomegalovirus (CMV) promoter or a PAX3–FOXO1-dependent super enhancer (cloned from the intronic *ALK* super enhancer; Supplementary Fig. S10A). This *ALK* super enhancer was consistent in FP-RMS cell lines and tumors, while completely absent in FN-RMS (Supplementary Fig. S3D). No activity was seen from the *ALK* super enhancer construct in FN-RMS cells lacking PAX3–FOXO1 (Supplementary Fig. S10B). The *ALK* super enhancer was suppressed by knockdown of PAX3–FOXO1 or by point mutation of the PAX3–FOXO1 binding motif (Supplementary Fig. S10C–S10E). BRD inhibition with JQ1 suppressed only the *ALK* super enhancer– but not the CMV-driven reporter in a dose-dependent manner *in vitro* (Fig. 7A), whereas the general transcription CDK7 inhibitor THZ1 suppressed both. Use of these reporter lines *in vivo* demonstrated a selective inhibition of PAX3–FOXO1 activity with subsequent significant suppression of tumor growth (Fig. 7B and C; Supplementary Fig. S10F). The tumor-suppressive activity of JQ1 was confirmed in a second FP-RMS cell line xenograft, SCMC (Supplementary Fig. S10G–S10H).

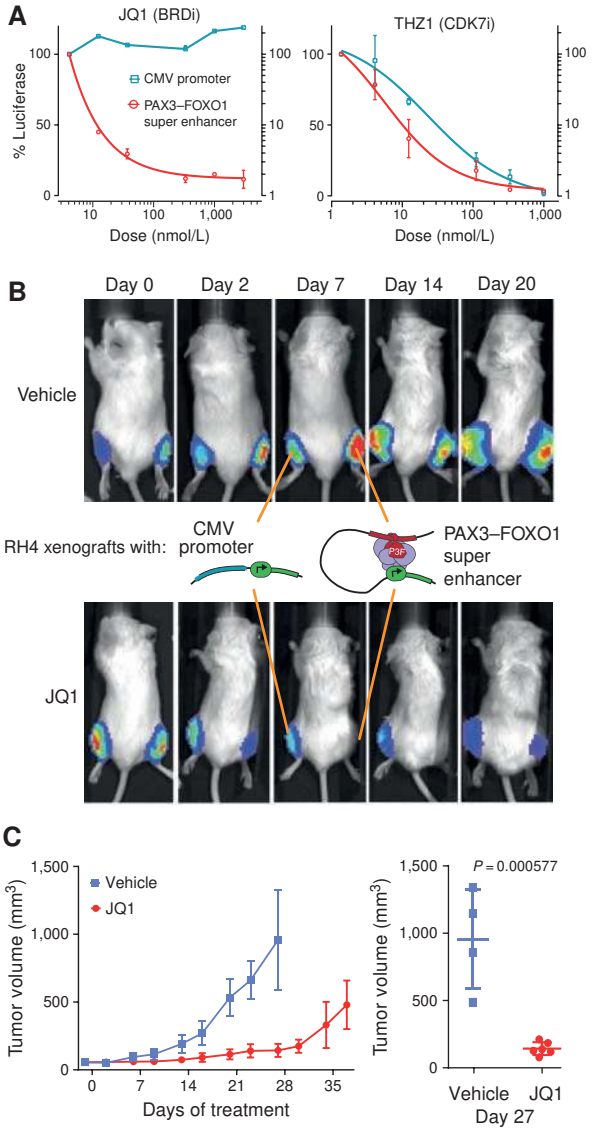


**Figure 7.** PAX3–FOXO1-dependent super enhancer disruption by BET inhibition *in vivo*. **A,** JQ1 selectively abolishes PAX3–FOXO1-dependent enhancer activity, as measured in PAX3–FOXO1 containing cells (RH4) stably transduced with a lentiviral pGreenFire reporter construct under the control of the PAX3–FOXO1-driven *ALK* super enhancer (SE), while not reducing the CMV-driven expression. CDK7 inhibitor THZ1 inhibits activity of both constructs. PAX3–FOXO1-driven luciferase (red line) is graphed on the left y-axis (linear), and CMV-driven luciferase (blue-green line) is graphed to the right y-axis (log 10 scale). Error bars show standard deviation of duplicate wells, and results are representative of 2 independent experiments. **B,** CMV (left flank) and *ALK* SE (right flank) reporter contructs in RH4 xenografts. JQ1 or vehicle treatment began on day 0 after the first image was taken. **C,** Left, RMS (RH4) tumor growth with vehicle- or JQ1-treated mice. Measurements were taken with caliper and include both CMV and PAX3–FOXO1-SE legs. Right, tumor volume at day 27. *P* value calculated by Welch unpaired *t* test.

## DISCUSSION

Pediatric sarcomas that harbor fusion oncogenes are reported with relatively few genomic alterations despite their clinically aggressive behavior (7). Here, we report that the *PAX3–FOXO1* fusion gene directs a profound epigenetic chromatin remodeling in cooperation with the master regulators MYOD, MYOG, and MYCN by the establishment of super enhancers.

By comprehensively charting the first epigenetic landscape of RMS in cell lines and primary tumors, we identified a core

commitment to super enhancer regulation of MYOD, MYOG, and MYCN, which in turn drive virtually all densely acetylated enhancer clusters that specify RMS cell identity. Although the concept of a "super" enhancer remains controversial, and may simply be a cluster of additive enhancers (24), we found the classification useful in that the most uniquely and highly expressed candidate MTFs were all driven by super enhancers, often more than one. Our results indicate that PAX3–FOXO1 directly establishes super enhancers to drive itself, *MYOD1*, and *MYCN*, and indirectly establishes a super enhancer (through MYOD and MYCN) to drive *MYOG*. Downstream, these factors are acting in concert, whereas in normal development they act sequentially (32). Virtually all of the discovered super enhancers were bound by 3 or 4 of these MTFs, and associated with the highest levels of gene expression. Remarkably, the presence of MYCN at these hyperactive regions resembles the function of MYC as a general transcriptional amplifier (29) and may underlie transcriptional addiction in FP-RMS (40). Together, these four MTFs cause a profound epigenetic reprogramming, freezing the cells in a myoblastic state with PAX3–FOXO1 as the conductor.

Cell type–specific distribution of BRD4 is accomplished by TF recruitment to their enhancers (41). Our study showed that PAX3–FOXO1 can direct *de novo* recruitment of BRD4 to specific chromatin sites when introduced into human fibroblasts, accompanied by opening of chromatin and acetylation of H3K27 at enhancers proximal to key RMS genes. This purely activating function of PAX3–FOXO1 in pediatric RMS is in sharp contrast to the dual functionality of EWS–FLI1 in pediatric Ewing sarcoma (5), which has both activating and repressive functions depending on genomic context.

The extent to which epigenetic profiling can aid prediction and interpretation of chemical sensitivities remains unclear. Using mechanistically informed drug screening, we observed that molecules targeted to super enhancer–bound coactivators (BRD4 and HDAC; ref. 22) and super enhancer targets (such as the receptor tyrosine kinases FGFR4 and ALK) are the most selectively potent in these FP-RMS cells. These data reinforce previous strategies that showed FP-RMS sensitivity to FGFR and IGF1R inhibition (42, 43) and HDAC inhibitors (4, 44, 45), and add previously unknown mechanistic insights to recently discovered BRD4 vulnerability (13). The observation that super enhancer–associated targets represent key vulnerabilities may be broadly applicable to cancers driven by epigenetic reprograming through super enhancer networks and may be critical to prioritizing combination strategies as well.

The same translocation which causes FP-RMS also creates an Achilles' heel by addicting cells to BRD4. Our data add to the pleiotropic utility of BRD4 inhibitors, with a recent wave of studies in a diverse group of cancers (37, 46–50). The transcriptional impact of BRD4 inhibition appears to be context dependent, where its antitumor effect is linked to dampening one or more master regulators, often including *MYC* in hematologic malignancies (51, 52), *MYCN* in neuroblastoma (37), *POU2AF1* and *PAX5* in DLBCL (47), or *FOSL1* in adenocarcinoma (53), among others. JQ1 was shown recently to be effective in reducing RMS tumor growth by antiangiogenic properties, but the underlying chromatin-based mechanisms or FP-RMS subtype selectivity were not explored (13). Here, we find BRDi caused selective downregulation of *MYC, MYCN, MYOD1, MYOG*, and many other downstream PAX3–FOXO1- and super enhancer–driven genes. Surprisingly, JQ1 did not decrease expression of *PAX3–FOXO1* mRNA at 6 hours, yet it rapidly decreased PAX3–FOXO1 protein stability. This may result from the disruption of interaction between BRD4 and PAX3–FOXO1, discovered by both coimmunoprecipitation and re-ChIP experiments, which JQ1 abrogated within hours of drug exposure. Thus, BRD inhibition by JQ1 leads to significant tumor suppression *in vitro* and *in vivo,* ablating the transcription-driving function of the fusion gene. Indeed, this mechanism may partially explain the antitumor effects seen with BI-2536 in FP-RMS mouse models (54), as this PLK1 inhibitor was recently found to possess a nanomolar inhibition of BET bromodomains (55). Excitingly, this provides a means of selectively drugging PAX3–FOXO1, a long-standing goal of FP-RMS research (56), and provides a new precision therapeutic for treatment of the aggressive PAX fusion–bearing RMS.

## METHODS

### Cell Lines and Primary Tumors

All cell lines were routinely tested for *Mycoplasma* within one or two passages of each experiment herein, and cell line identities have been ensured by RNA-seq and genotyping. RH4, RH3, RH5, and RH41 were kind gifts from Dr. Peter Houghton (obtained between 2008 and 2010), SCMC from Dr. Janet Shipley (obtained between 2013 and 2015), and RD, CTR, and Birch from Dr. Lee Helman (obtained between 2008 and 2010). CRL7250 and NIH3T3 were obtained from the ATCC (obtained between 2008 and 2010). Validation was performed by DNA fingerprinting AmpFlSTR Identifiler PCR Amplification Kit (Catalog Number 4322288) by Life Technologies. Cell lines were grown in DMEM, 10% FBS, and supplemented with penicillin/streptomycin. Primary RMS cultures established from patient-derived tumor xenografts were collected at the St. Jude Children's Research Hospital (57). Cells were maintained in Neurobasal-A medium (ThermoFisher Scientific) supplemented with 2xB-27 supplement (ThermoFisher Scientific), 20 ng/mL bFGF, and 20 ng/mL EGF (both from PeproTech), and cultured on gelatin-coated plates in 5% $CO_2$ at 37°C. Primary tumors were acquired via the NCI-coordinated ClinOmics protocol as previously described (58).

### ChIP-seq and RNA-seq

ChIP-seq (59) and RNA-seq (3) were performed as previously described. Raw sequencing data and processed files have been made available through Gene Expression Omnibus (GEO) SuperSeries accession number GSE83728, which is comprised of SubSeries accession numbers GSE83724, GSE83725, GSE83726, and GSE83727. Details, including Illumina sequencing and bioinformatic methods, are available in Supplementary Methods.

### DNase-seq with 10,000 Cells

Sites of DNase-sensitive chromatin were captured from 10,000 cells as recently described (60) with slight modifications. Briefly, freshly trypsinized cells were resuspended in DMEM, counted in duplicate (Nexcelom Automated Cell Counter), pelleted and resuspended in lysis buffer to achieve 120 µL of 60K cells, which was then divided into 6 replicates (10K cells per tube). DNaseI (Roche 04-716-728-001) was added to the cells (0.25–0.5 units) and incubated for 5 minutes at 37°C. The digestion was halted with 50 µL of stop buffer (9.5 mL $H_2O$ + 100 µL 1M TrisHCl pH 7.4 + 20 µL 5 mol/L NaCl + 200 µL 0.5 mol/L EDTA, with 150 µL 10% SDS and 125 µL proteinase K added just before use). Proteinase K activation at 55°C for 1 hour was followed by DNA purification by column (MiniElute PCR

purification kit, Qiagen). Library preparation was performed as with ChIP-seq samples, except that paired-end was used rather than single-end sequencing on the NextSeq 500 (Illumina).

### Small-Molecule Compounds

All molecules were dissolved in DMSO to a final concentration of 10 mmol/L and diluted to a final DMSO concentration of <0.03% by volume in DMEM for cell culture experiments. JQ1 was a gift from Jay Bradner (Novartis) and Jun Qi (Dana-Farber Cancer Institute). Bromosporine was provided by Peter Brown of the Structural Genomics Consortium. THZ1 was supplied by Nat Gray (Dana-Farber Cancer Institute). Other bromodomain inhibitors (OTX015, I-Bet-151, I-Bet-762, and I-Bet-726) were generously supplied by the Developmental Therapeutics Program (NCI, NIH).

### Time Course of Dose-Response Cell Growth Assay

Dose responses were performed by quantifying percent cell confluence from phase contrast images taken every 4 hours using the IncuCyte ZOOM in 384-well plate format. Dose response was achieved using a range of 12 concentrations from 30 μmol/L to 0.17 nmol/L (dilutions divided by 3) and were performed in triplicate. Cells were plated to achieve 15% confluence at time of drug dosing, and monitored until control (DMSO) wells reached >95% confluence. $IC_{50}$ values were calculated for each time point using the R statistical package drc (https://cran.r-project.org/web/packages/drc/drc.pdf).

### Luciferase-Expressing Cells

pGreenFire vector from Systems Biosciences was modified by insertion of a *cis*-regulatory element surrounding the PAX3–FOXO1 binding site within the super enhancer found within the intronic region of the ALK gene (chr2:29880537–29880842). Cloning was performed using pCR2.1–TOPO system from PCR amplification product from genomic DNA of RH4 FP-RMS cells, and shuttled into the pGF1 vector at the EcoRI restriction site upstream of a minimal CMV promoter, which was completely inactive on its own in RMS cell lines. Viral particles were produced in HEK293T cells, harvested, filtered, and pelleted. pGF1 cloning vectors developed at SBI are self-inactivating as a result of a deletion in the U3 region of 3′-LTR. Upon integration into the genome, the 5′ LTR promoter is inactivated, which prevents formation of replication-competent viral particles. Pooled cells were selected using puromycin.

### Animal Studies

Animal studies were approved by the National Cancer Institute's Animal Care and Use Committee, and all animal care was in accordance with institutional guidelines. Complete details are reported in Supplementary Methods.

## Disclosure of Potential Conflicts of Interest

No potential conflicts of interest were disclosed.

## Authors' Contributions

**Conception and design:** B.E. Gryder, M.E. Yohe, H.-C. Chou, J.S. Wei, C.J. Thomas, J. Khan
**Development of methodology:** B.E. Gryder, H.-C. Chou, Y. Song, R. Rota, X. Wen, S. Sindiri, M. Ferrer, J.F. Shern, C.J. Thomas, J. Khan
**Acquisition of data (provided animals, acquired and managed patients, provided facilities, etc.):** B.E. Gryder, M.E. Yohe, X. Zhang, J. Marques, M. Wachtel, N. Sen, Y. Song, R. Rota, X. Wen, J.S. Wei, F.G. Barr, S. Das, T. Andresson, M. Lal-Nag, M. Ferrer, C.J. Thomas, J. Khan
**Analysis and interpretation of data (e.g., statistical analysis, biostatistics, computational analysis):** B.E. Gryder, H.-C. Chou, J. Marques, M. Wachtel, B. Schaefer, N. Sen, A. Cleveland, X. Wen, S. Sindiri, J.S. Wei, F.G. Barr, R. Guha, M. Lal-Nag, M. Ferrer, J.F. Shern, K. Zhao, C.J. Thomas, J. Khan
**Writing, review, and/or revision of the manuscript:** B.E. Gryder, M.E. Yohe, H.-C. Chou, B. Schaefer, N. Sen, R. Rota, J.S. Wei, F.G. Barr, R. Guha, M. Ferrer, J.F. Shern, K. Zhao, C.J. Thomas, J. Khan
**Administrative, technical, or material support (i.e., reporting or organizing data, constructing databases):** B.E. Gryder, H.-C. Chou, X. Wen, J. Khan
**Study supervision:** R. Rota, C.J. Thomas, J. Khan
**Other (writing original manuscript):** B.E. Gryder
**Other (wet-lab investigation, providing materials):** A. Gualtieri, S. Pomella

## Acknowledgments

The authors are very grateful to C. Thiele, B. Stanton, J. Waterfall, L. Cao, T. Misteli, and C. Vakoc for helpful discussions and review of the manuscript. We are thankful to J. Qi, J. Bradner, N. Gray, P. Brown, the Structural Genomics Consortium, and the Developmental Therapeutics Program (NCI, NIH) for providing small molecules. We also appreciate the help of S. Li, N. Shivaprasad, S. Michael, and M. Skarzynski in providing reagents, cell lines, and antibodies. We thank C. Lin and R. Patidar for sharing scripts and bioinformatic advice.

## Grant Support

This project has been funded with federal funds from the National Cancer Institute, NIH, contract no. HHSN261200800001E. A. Gualtieri is a recipient of a Fondazione Veronesi fellowship. R. Rota has been supported by Associazione Italiana Ricerca sul Cancro (AIRC) and PE-2013-02355271.

The content of this publication does not necessarily reflect the views or policies of the Department of Health and Human Services, nor does mention of trade names, commercial products, or organizations imply endorsement by the U.S. government. Frederick National Laboratory is accredited by AAALAC International and follows the Public Health Service Policy for the Care and Use of Laboratory Animals. Animal care was provided in accordance with the procedures outlined in the "Guide for Care and Use of Laboratory Animals" (National Research Council, 2011; National Academies Press, Washington, DC).

Received November 19, 2016; revised March 20, 2017; accepted April 21, 2017; published OnlineFirst April 26, 2017.

## REFERENCES

1. Lee Tong I, Young Richard A. Transcriptional regulation and its misregulation in disease. Cell 2013;152:1237–51.
2. Rabbitts T. Chromosomal translocations in human cancer. Nature 1994;372:143–9.
3. Shern JF, Chen L, Chmielecki J, Wei JS, Patidar R, Rosenberg M, et al. Comprehensive genomic analysis of rhabdomyosarcoma reveals a landscape of alterations affecting a common genetic axis in fusion-positive and fusion-negative tumors. Cancer Discov 2014;4:216–31.
4. Chen X, Stewart E, Shelat Anang A, Qu C, Bahrami A, Hatley M, et al. Targeting Oxidative Stress in Embryonal Rhabdomyosarcoma. Cancer Cell 2013;24:710–24.
5. Riggi N, Knoechel B, Gillespie Shawn M, Rheinbay E, Boulay G, Suvà Mario L, et al. EWS-FLI1 utilizes divergent chromatin remodeling mechanisms to directly activate or repress enhancer elements in ewing sarcoma. Cancer Cell 2014;26:668–81.
6. Kadoch C, Crabtree Gerald R. Reversible Disruption of mSWI/SNF (BAF) Complexes by the SS18-SSX oncogenic fusion in synovial sarcoma. Cell 2013;153:71–85.
7. Pizzo PA, Poplack DG. Principles and practice of pediatric oncology. Philadelphia: Lippincott Williams & Wilkins; 2015.

8. Missiaglia E, Williamson D, Chisholm J, Wirapati P, Pierron G, Petel F, et al. PAX3/FOXO1 fusion gene status is the key prognostic molecular marker in rhabdomyosarcoma and significantly improves current risk stratification. J Clin Oncol 2012;30:1670–7.
9. Khan J, Simon R, Bittner M, Chen Y, Leighton SB, Pohida T, et al. Gene expression profiling of alveolar rhabdomyosarcoma with cDNA microarrays. Cancer Res 1998;58:5009–13.
10. Davis RJ, Barr FG. Fusion genes resulting from alternative chromosomal translocations are overexpressed by gene-specific mechanisms in alveolar rhabdomyosarcoma. Proc Nat Acad Sci 1997;94:8047–51.
11. Davicioni E, Graf Finckenstein F, Shahbazian V, Buckley JD, Triche TJ, Anderson MJ. Identification of a PAX-FKHR gene expression signature that defines molecular classes and determines the prognosis of alveolar rhabdomyosarcomas. Cancer Res 2006;66:6936–46.
12. Khan J, Bittner ML, Saal LH, Teichmann U, Azorsa DO, Gooden GC, et al. cDNA microarrays detect activation of a myogenic transcription program by the PAX3–FKHR fusion oncogene. Proc Natl Acad Sci U S A 1999;96:13264–9.
13. Bid HK, Phelps DA, Xiao L, Guttridge DC, Lin J, London C, et al. The bromodomain BET inhibitor JQ1 suppresses tumor angiogenesis in models of childhood sarcoma. Mol Cancer Ther 2016;15:1018–28.
14. Barr FG, Galili N, Holick J, Biegel JA, Rovera G, Emanuel BS. Rearrangement of the PAX3 paired box gene in the paediatric solid tumour alveolar rhabdomyosarcoma. Nat Genet 1993;3:113–7.
15. Cao LA, Yu YK, Bilke S, Walker RL, Mayeenuddin LH, Azorsa DO, et al. Genome-Wide Identification of PAX3–FKHR binding sites in rhabdomyosarcoma reveals candidate target genes important for development and cancer. Cancer Res 2010;70:6497–508.
16. Roadmap Epigenomics C, Kundaje A, Meuleman W, Ernst J, Bilenky M, Yen A, et al. Integrative analysis of 111 reference human epigenomes. Nature 2015;518:317–30.
17. McLean CY, Bristor D, Hiller M, Clarke SL, Schaar BT, Lowe CB, et al. GREAT improves functional interpretation of cis-regulatory regions. Nat Biotechnol 2010;28:495–501.
18. Begum S, Emani N, Cheung A, Wilkins O, Der S, Hamel PA. Cell-type-specific regulation of distinct sets of gene targets by Pax3 and Pax3//FKHR 2005;24:1860–72.
19. Rao Suhas SP, Huntley Miriam H, Durand Neva C, Stamenova Elena K, Bochkov Ivan D, Robinson James T, et al. A 3D map of the human genome at kilobase resolution reveals principles of chromatin looping. Cell 2014;159:1665–80.
20. Trapnell C, Cacchiarelli D, Grimsby J, Pokharel P, Li S, Morse M, et al. The dynamics and regulators of cell fate decisions are revealed by pseudotemporal ordering of single cells. Nat Biotech 2014;32:381–6.
21. Tenente IM, Hayes MN, Ignatius MS, McCarthy K, Yohe M, Sindiri S, et al. Myogenic regulatory transcription factors regulate growth in rhabdomyosarcoma. eLife 2017;6:e19214.
22. Hnisz D, Abraham Brian J, Lee Tong I, Lau A, Saint-André V, Sigova Alla A, et al. Super-enhancers in the control of cell identity and disease. Cell 2013;155:934–47.
23. Whyte WA, Orlando DA, Hnisz D, Abraham BJ, Lin CY, Kagey MH, et al. Master transcription factors and mediator establish super-enhancers at key cell identity genes. Cell 2013;153:307–19.
24. Dukler N, Gulko B, Huang Y-F, Siepel A. Is a super-enhancer greater than the sum of its parts? Nat Genet 2017;49:2–3.
25. Lin CY, Erkek S, Tong Y, Yin L, Federation AJ, Zapatka M, et al. Active medulloblastoma enhancers reveal subgroup-specific cellular origins. Nature 2016;530:57–62.
26. Davis RL, Weintraub H, Lassar AB. Expression of a single transfected cDNA converts fibroblasts to myoblasts. Cell 1987;51:987–1000.
27. Ernst J, Kheradpour P, Mikkelsen TS, Shoresh N, Ward LD, Epstein CB, et al. Mapping and analysis of chromatin state dynamics in nine human cell types. Nature 2011;473:43–9.
28. Orlando David A, Chen Mei W, Brown Victoria E, Solanki S, Choi Yoon J, Olson Eric R, et al. Quantitative ChIP-Seq normalization reveals global modulation of the epigenome. Cell Reports 2014;9:1163–70.
29. Lin Charles Y, Lovén J, Rahl Peter B, Paranal Ronald M, Burge Christopher B, Bradner James E, et al. Transcriptional amplification in tumor cells with elevated c-myc. Cell 2012;151:56–67.
30. Nie Z, Hu G, Wei G, Cui K, Yamane A, Resch W, et al. c-Myc is a universal amplifier of expressed genes in lymphocytes and embryonic stem cells. Cell 2012;151:68–79.
31. Saint-André V, Federation AJ, Lin CY, Abraham BJ, Reddy J, Lee TI, et al. Models of human core transcriptional regulatory circuitries. Genome Res 2016;26:385–96.
32. Hettmer S, Wagers AJ. Muscling in: Uncovering the origins of rhabdomyosarcoma. Nat Med 2010;16:171–3.
33. Kitamura T, Feng Y, Kitamura YI, Chua SC, Xu AW, Barsh GS, et al. Forkhead protein FoxO1 mediates Agrp-dependent effects of leptin on food intake. Nature medicine 2006;12:534–40.
34. Shi J, Vakoc Christopher R. The mechanisms behind the Therapeutic Activity of BET Bromodomain Inhibition. Mol Cell 2014;54:728–36.
35. Jones LH, Bunnage ME. Applications of chemogenomic library screening in drug discovery. Nat Rev Drug Discov 2017;16:285–96.
36. Filippakopoulos P, Qi J, Picaud S, Shen Y, Smith WB, Fedorov O, et al. Selective inhibition of BET bromodomains. Nature 2010;468:1067–73.
37. Puissant A, Frumm SM, Alexe G, Bassil CF, Qi J, Chanthery YH, et al. Targeting MYCN in neuroblastoma by BET bromodomain inhibition. Cancer Discovy 2013;3:308–23.
38. Jang MK, Mochizuki K, Zhou M, Jeong H-S, Brady JN, Ozato K. The bromodomain protein Brd4 Is a positive regulatory component of P-TEFb and stimulates RNA polymerase II-dependent transcription. Mol Cell 2005;19:523–34.
39. Lovén J, Hoke Heather A, Lin Charles Y, Lau A, Orlando David A, Vakoc Christopher R, et al. Selective inhibition of tumor oncogenes by disruption of super-enhancers. Cell 2013;153:320–34.
40. Bradner JE, Hnisz D, Young RA. Transcriptional addiction in cancer. Cell 2017;168:629–43.
41. Roe J-S, Mercan F, Rivera K, Pappin Darryl J, Vakoc Christopher R. BET bromodomain inhibition suppresses the function of hematopoietic transcription factors in acute myeloid leukemia. Mol Cell 2015;58:1028–39.
42. Crose LE, Etheridge KT, Chen C, Belyea B, Talbot LJ, Bentley RC, et al. FGFR4 blockade exerts distinct antitumorigenic effects in human embryonal versus alveolar rhabdomyosarcoma. Clin Cancer Res 2012;18:3780–90.
43. Kim SY, Toretsky JA, Scher D, Helman LJ. The role of IGF-1R in pediatric malignancies. Oncologist 2009;14:83–91.
44. Abraham J, Nuñez-Álvarez Y, Hettmer S, Carrió E, Chen H-IH, Nishijo K, et al. Lineage of origin in rhabdomyosarcoma informs pharmacological response. Genes Deve 2014;28:1578–91.
45. Kutko MC, Glick RD, Butler LM, Coffey DC, Rifkind RA, Marks PA, et al. Histone deacetylase inhibitors induce growth suppression and cell death in human rhabdomyosarcoma in vitro. Clin Cancer Res 2003;9:5749–55.
46. Asangani IA, Dommeti VL, Wang X, Malik R, Cieslik M, Yang R, et al. Therapeutic targeting of BET bromodomain proteins in castration-resistant prostate cancer. Nature 2014;510:278–82.
47. Chapuy B, McKeown Michael R, Lin Charles Y, Monti S, Roemer Margaretha GM, Qi J, et al. Discovery and characterization of super-enhancer-associated dependencies in diffuse large B cell lymphoma. Cancer cell 2013;24:777–90.
48. Dawson MA, Prinjha RK, Dittmann A, Giotopoulos G, Bantscheff M, Chan WI, et al. Inhibition of BET recruitment to chromatin as an effective treatment for MLL-fusion leukaemia. Nature 2011;478:529–33.
49. De Raedt T, Beert E, Pasmant E, Luscan A, Brems H, Ortonne N, et al. PRC2 loss amplifies Ras-driven transcription and confers sensitivity to BRD4-based therapies. Nature 2014;514:247–51.
50. Zuber J, Shi JW, Wang E, Rappaport AR, Herrmann H, Sison EA, et al. RNAi screen identifies Brd4 as a therapeutic target in acute myeloid leukaemia. Nature 2011;478:524–U124.

51. Delmore Jake E, Issa Ghayas C, Lemieux Madeleine E, Rahl Peter B, Shi J, Jacobs Hannah M, et al. BET bromodomain inhibition as a therapeutic strategy to target c-Myc. Cell 2011;146:904–17.
52. Rathert P, Roth M, Neumann T, Muerdter F, Roe J-S, Muhar M, et al. Transcriptional plasticity promotes primary and acquired resistance to BET inhibition. Nature 2015;525:543–7.
53. Lockwood WW, Zejnullahu K, Bradner JE, Varmus H. Sensitivity of human lung adenocarcinoma cell lines to targeted inhibition of BET epigenetic signaling proteins. Proc Nat Acad Sci 2012;109:19408–13.
54. Thalhammer V, Lopez-Garcia LA, Herrero-Martin D, Hecker R, Laubscher D, Gierisch ME, et al. PLK1 Phosphorylates PAX3–FOXO1, the inhibition of which triggers regression of alveolar rhabdomyosarcoma. Cancer Res 2015;75:98–110.
55. Ciceri P, Müller S, O'Mahony A, Fedorov O, Filippakopoulos P, Hunt JP, et al. Dual kinase-bromodomain inhibitors for rationally designed polypharmacology. Nat Chem Biol 2014;10:305–12.
56. Linardic CM.PAX3–FOXO1 fusion gene in rhabdomyosarcoma. Cancer Lett 2008;270:10–8.
57. Stewart E, Federico S, Karlstrom A, Shelat A, Sablauer A, Pappo A, et al. The childhood solid tumor network: a new resource for the developmental biology and oncology research communities. Devel Biol 2016;411:287–93.
58. Chang W, Brohl A, Patidar R, Sindiri S, Shern JF, Wei JS, et al. Multidimensional clinomics for precision therapy of children and adolescent young adults with relapsed and refractory cancer: a report from the Center for Cancer Research. Clin Cancer Res 2016;22:3810–20.
59. Barski A, Cuddapah S, Cui K, Roh T-Y, Schones DE, Wang Z, et al. High-resolution profiling of histone methylations in the human genome. Cell 2007;129:823–37.
60. Jin W, Tang Q, Wan M, Cui K, Zhang Y, Ren G, et al. Genome-wide detection of DNase I hypersensitive sites in single cells and FFPE tissue samples. Nature 2015;528:142–6.